

Characterization of Viral Capsid Protein Self-Assembly around Short Single-Stranded RNA

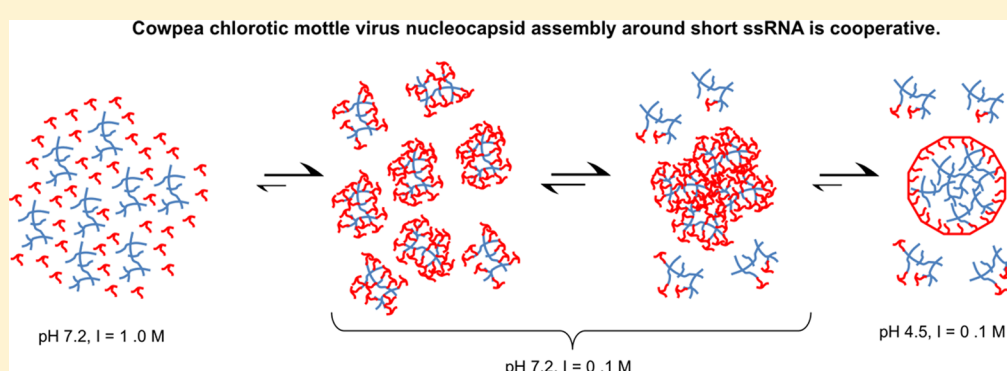
Mauricio Comas-Garcia,^{†,||} Rees F. Garmann,[†] Surendra W. Singaram,^{†,§} Avinoam Ben-Shaul,[§] Charles M. Knobler,[†] and William M. Gelbart^{*,†,‡}

[†]Department of Chemistry and Biochemistry, University of California, Los Angeles, California 90095, United States

[‡]California NanoSystems Institute, University of California, Los Angeles, California 90095, United States

[§]Department of Physical Chemistry, The Hebrew University, Jerusalem 91904, Israel

Supporting Information



ABSTRACT: For many viruses, the packaging of a single-stranded RNA (ss-RNA) genome is spontaneous, driven by capsid protein–capsid protein (CP) and CP–RNA interactions. Furthermore, for some multipartite ss-RNA viruses, copackaging of two or more RNA molecules is a common strategy. Here we focus on RNA copackaging *in vitro* by using cowpea chlorotic mottle virus (CCMV) CP and an RNA molecule that is short (500 nucleotides (nts)) compared to the lengths (\approx 3000 nts) packaged in wild-type virions. We show that the degree of cooperativity of virus assembly depends not only on the relative strength of the CP–CP and CP–RNA interactions but also on the RNA being short: a 500-nt RNA molecule cannot form a capsid by itself, so its packaging requires the aggregation of multiple CP–RNA complexes. By using fluorescence correlation spectroscopy (FCS), we show that at neutral pH and sufficiently low concentrations RNA and CP form complexes that are smaller than the wild-type capsid and that four 500-nt RNAs are packaged into virus-like particles (VLPs) only upon lowering the pH. Further, a variety of bulk-solution techniques confirm that fully ordered VLPs are formed only upon acidification. On the basis of these results, we argue that the observed high degree of cooperativity involves equilibrium between multiple CP/RNA complexes.

INTRODUCTION

Understanding how single-stranded (ss) RNA genomes and capsid proteins (CPs) interact *in vivo* to form nucleocapsids during a viral infection is a highly challenging task. Beyond playing a direct role in packaging the genome, CP has also been implicated in suppression of RNA silencing and in controlling minus- and plus-strand RNA synthesis in the host cell.¹ Extensive work has been done on *in vitro* packaging of viral and nonviral RNAs by CP, a spontaneous process shown to be driven by CP–CP and CP–RNA interactions, consistent with the facts that virally encoded enzymes are not involved in many instances of ssRNA packaging and that empty capsids are generally not formed during an infection. These studies have highlighted the importance of both specific and nonspecific interactions that give rise to virus assembly.^{2–9}

In an effort to understand how such interactions direct cowpea chlorotic mottle virus (CCMV) virion assembly, we have previously focused on how the size of the packaged RNA

affects the size of the nucleocapsid and its efficiency of formation.^{7,8} We have shown that CCMV CP can spontaneously self-assemble around viral (homologous and heterologous) and virally derived RNAs ranging in length from 140 to 12 000 nucleotides (nts).⁷ In particular, if the RNA is significantly shorter (\leq 1000 nts), then the 3200-nt wild-type (WT) several RNAs are packaged in a single capsid, such that the total RNA content is similar to that of the WT virus.

These *in vitro* results for short RNAs are consistent with the *in vivo* copackaging of RNAs 3 (\approx 2200 nts) and 4 (\approx 800 nts) in the case of the *Bromovirus* genus. In fact, among multipartite ssRNA viruses, copackaging of two or more RNA molecules is a very common strategy, which in some cases leads to packaging of subgenomic RNAs that are not necessary for infection.^{10,11}

Received: March 27, 2014

Revised: June 13, 2014

Published: June 16, 2014

However, to date, little is known about the mechanism(s) that lead to multiple RNAs being packaged in a single capsid, mainly because during the course of an infection it is almost impossible to uncouple RNA replication from capsid assembly.^{10–12} (For *in vitro* studies of copackaging, see the work of Fox et al.¹³ with CCMV CP and RNAs 3 and 4, in which the dependence of copackaging efficiency on RNA composition is measured.) In the present study, we examine RNA copackaging *in vitro* by using CCMV CP and a 500-nt-long RNA. Our measurements are aimed at understanding—in the simplest experiments and in the absence of any specific RNA–CP interactions—how short equal-length RNAs can be copackaged by CCMV CP.

We find that, unlike the case for longer RNAs,^{7,8,14} the self-assembly of CCMV CP around 500-nt RNAs is highly cooperative; i.e., at CP:RNA mass ratios smaller than the minimum needed to package all of the RNA, there are only two species in solution: CP-bound single molecules of RNA and RNA–CP complexes consisting of several RNAs bound to CP. More explicitly, by using gel electrophoretic mobility assays (EMAs), velocity sedimentation, single-molecule fluorescence correlation spectroscopy (sm-FCS), and cryo-electron microscopy, we show that at neutral pH RNA and CP form amorphous complexes; the number of such RNA–CP complexes that aggregate to form *protocapsids* depends on the absolute RNA concentration; that fully formed, ordered, *nucleocapsids* [virus-like particles (VLPs)] are formed only upon acidification; and that four 500-nt RNAs are packaged into each VLP. On the basis of these results, we argue that the cooperativity shown by short RNAs is a consequence of the equilibrium between multiple-RNA CP/RNA complexes (MRCs) and single-RNA CP/RNA complexes, i.e., of the aggregation of single-RNA CP-bound complexes into MRCs.

METHODS AND MATERIALS

Materials. Restriction enzymes were obtained from New England Biolabs and were used as recommended by the manufacturer. T7 RNA polymerase was a gift from Prof. Feng Guo (Dept. of Biological Chemistry, UCLA). Enzymes and all other reagents used were DNase-, RNase-, and protease-free.

PCR Amplification of DNA Templates. The DNA template needed for *in vitro* transcription of the 500-nt RNA was obtained by PCR of the first 500 bp of the pT7B1 plasmid.¹⁵ B1 refers here to the first gene of the brome mosaic virus (BMV); we used a 5' primer d(TAATACGACTCACTATAGGTAGACCACGGAACGAGGTTC) (T7 promoter is underlined) and d(CACATCCTCTCCTCATGTC) as a reverse primer. The template was purified by standard procedures.¹⁶

RNA Transcription and Fluorescence Labeling. The DNA template was transcribed with T7 RNA polymerase and labeled with ChromaTide Alexa Fluor 488–5-UTP (AF488) (Life Technologies). This modified rUTP is randomly incorporated during transcription, using 600:600:600:5.32:1 molar ratios of rATP:rGTP:rCTP:rUTP:modified-rUTP, giving a density of labeling around 0.5. The label density for the RNA was calculated by linear regression of a calibration curve of pure AF488–rUTPs. The fluorescence measurements were carried out with a QuantaMaster Spectrofluorimeter (Photon Technology International) in a 40 μL quartz cuvette (Sterna Cells). Fluorescent RNAs were always kept in the dark in amber tubes, and room light was minimized during handling.

CCMV CP Purification. CCMV was purified from infected California cowpea plant (*Vigna unguiculata* cv Black eye pea),¹⁷

and CP was isolated as described by Annamalai and Rao.⁴ SDS-PAGE and MALDI-TOF were employed to ascertain that the purified protein was intact.

CCMV CP Labeling. Alexa Fluor-647 succinimidyl ester (AF647) (Life Technologies) was covalently linked to solvent-exposed lysines on the exterior surface of CCMV virions.¹⁸ CCMV was concentrated to 5 mg/mL and then dialyzed overnight at 4 °C against 0.1 M HEPES pH 7.2 and 5 mM MgCl₂. The dye-conjugation reaction was carried out at room temperature for 2 h by mixing the virus with AF647 (10 mg/mL) at an AF647:CCMV (virion) mass ratio of 0.005 [AF647:CCMV (virion) molar ratio of 18.4:1] and then dialyzing against the virus suspension buffer (VSB: 50 mM sodium acetate, 8 mM magnesium acetate, pH 4.5) overnight at 4 °C. A sucrose cushion was used to purify the sample from the unreacted dye: 2.5 mL of sample plus 0.5 mL of 10% sucrose in VSB were centrifuged for 2 h at 100 000 rpm and 4 °C in a TLA 110 rotor; the supernatant was then discarded and the pellet resuspended with VSB and stored at –80 °C. The density of labeling (DOL), defined as the fraction of CPs labeled by AF647, was determined before and after CP purification from the UV-vis absorbance using Beer's law: DOL = Abs₆₅₀MW/[CP] ϵ_{650} , where Abs₆₅₀ is the absorbance maximum, MW is the molecular weight of the CCMV CP (20.3 kDa), [CP] is the CP concentration in mg/mL, and ϵ_{650} is the molar extinction coefficient of the dye (239 000 M^{–1} cm^{–1}). These conditions were optimized to achieve DOL = 0.07, which allowed maximum CP recovery after virion disassembly.

In vitro Assemblies. Unless otherwise stated, the RNA concentration in every reaction was 30 ng/ μL (150 nM RNA). We followed two different assembly protocols: one- and two-step dialysis. For both protocols, the first step was to mix the CP and RNA in buffer B (1 M NaCl, 20 mM Tris, pH 7.2, 1 mM EDTA, 1 mM DTT, and 1 mM PMSF). For the one-step assembly, the samples were then dialyzed for 24 h at 4 °C against the RNA assembly buffer (RAB: 50 mM NaCl, 10 mM KCl, 5 mM MgCl₂, 1 mM DTT, 50 mM Tris, pH 7.2). For the two-step assembly, a 12 h dialysis against RAB was followed by a 12 h dialysis against VSB. All reactions were carried out at 4 °C and protected from the light.

Electrophoretic Mobility Analysis (EMA). After each assembly, a 10 μL aliquot of each sample was mixed with 3 μL of glycerol and loaded into a 1% agarose gel (EMD OmniPur) in virus electrophoresis buffer (0.1 M sodium acetate, 1 mM EDTA, pH 5.5). The samples were electrophoresed at 4 °C for 1.25 h at 65 V in a horizontal gel apparatus (Fisher) and stained with a solution of 5 $\mu\text{g}/\text{mL}$ ethidium bromide. The gels were visualized with an FX Pro Plus Fluorimager/PhosphorImager (Bio-Rad) by exciting AF647, AF488, and ethidium bromide.

Single-Molecule Fluorescence Correlation Spectroscopy (sm-FCS). sm-FCS measurements were performed using a confocal microscope (Olympus IX71). Emission lines at 488 and 637 nm of a continuous-wave argon-ion laser (IonLaser Technology, Frankfort, IL) were used as excitation sources. The details of the experimental setup are described elsewhere.¹⁹ The excitation volume was of the order of 1 fL, and before and after every experiment, it was determined by measuring the diffusion coefficient of a purified sample of fluorescently labeled 500-nt RNA VLPs (AF488–RNA and AF647–CP) at the same concentration as the samples. The fluorescence signal was detected by two avalanche photodiodes (APDs, AQR-14, PerkinElmer Inc.). Detected photon pulses were sent to a hardware correlator card (ALV-60010, ALV GmbH, Langen,

Germany), which computed the cross-correlation of the two channels with a temporal resolution of 6.5 ns. A detailed description of the theoretical analysis of sm-FCS data is found in the Supporting Information.

sm-FCS Sample Preparation and Measurements. For CP:RNA titration curves, the samples were diluted from 150 nM RNA to 10 nM in a single step. To avoid nonspecific adsorption, the buffers (either RAB or VSB) used for dilutions contained 0.05% (v/v) Tween-20. All measurements were performed at room temperature, and each sample was measured 40 times with a 10 s acquisition time per run. The data were analyzed by two methods: by nonlinear least-squares fitting for each run, taking the average of the fitting parameters for the 40 runs, and by first averaging all the $G(\tau)$'s and then by a nonlinear least-squares fitting of the data, using the standard deviation of the average $G(\tau)$ as the instrumental error. The methods gave similar results, and the quality of the fitting procedures was comparable. The data were analyzed with QtiPlot data analysis software (ProIndep Serv).

Velocity Centrifugation in Sucrose Gradients. Each sucrose gradient was prepared by adding 5.2 mL of a 20% sucrose solution in the desired buffer (RAB or VSB) to a thin-wall tube for a SW 50.1 rotor (Beckman Coulter). The tubes were balanced, parafilmmed, and frozen at -80°C for 1 h and then thawed at 4°C for 2 h and refrozen. This freezing–thawing cycle was repeated twice more, resulting in reproducible 10–40% sucrose gradients. The gradients were loaded with 0.2 mL of the sample, rebalanced, and centrifuged for 3 h at 30 000 rpm at 4°C and then manually fractionated by taking 0.2 mL aliquots from top to bottom. The pipet tip was changed after collecting each fraction. The 26 extracted fractions were loaded into a 96-well flat-bottom plate, and the fluorescence intensities for the CP and the RNA (AF647 and AF488) were measured for each fraction using a Tecan M1000 plate reader.

Cryo-EM Imaging. Cryo-EM samples were prepared by depositing 3 μL of assembly reaction mixture on a Quantifoil holey carbon grid (200 mesh; R2/1) that had previously been glow-discharged. The grids were then blotted and flash-frozen by rapid plunging into a liquid ethane bath cooled to liquid nitrogen temperature. Micrographs were acquired using the FEI Tecnai G2 TF20 microscope operated at an accelerating voltage of 200 kV. Total beam exposure was maintained between 30 and 50 e/ \AA^2 . Images were recorded at 3–4 μm underfocus with a TIETZ F415MP 4k \times 4k pixel CCD camera.

RESULTS

RNA and CP Fluorescence Labeling Does Not Affect *in vitro* Assembly. To examine how fluorescence labeling of CP and RNA affected the assembly process, we carried out separate assemblies at different ratios of AF647-labeled to unlabeled CP around both AF488-labeled and unlabeled 500-nt RNA, and unlabeled RNA. EMAs and negative-stain electron micrographs confirmed that VLP formation is not affected by varying the ratios of labeled to unlabeled CP with either labeled or unlabeled RNA (data not shown). The electrophoretic mobility of AF647-labeled VLPs was distinguishable from that of unlabeled VLPs only when CP DOL ≥ 0.05 (data not shown). It has been reported¹⁸ that binding of fluorophores to CCMV at high DOLs leads to a substantial increase in their diameter, but negative-stain EMs show that at the low densities we employed the diameter of the modified virions is

indistinguishable from those assembled with unlabeled RNA (data not shown).

Assembly of CCMV CP around 500-nt RNA Is Highly Cooperative. In previous studies, we have shown that the interaction of CCMV CP around RNA at neutral pH and low ionic strength leads to disordered CP–RNA complexes in which the RNA is subject to attack by RNase.⁹ It is only when the pH is lowered that regular, protective VLPs are formed. That this is the case in assemblies around the 500-nt RNA examined here can be seen in the cryo-EM images shown in Figure 1.

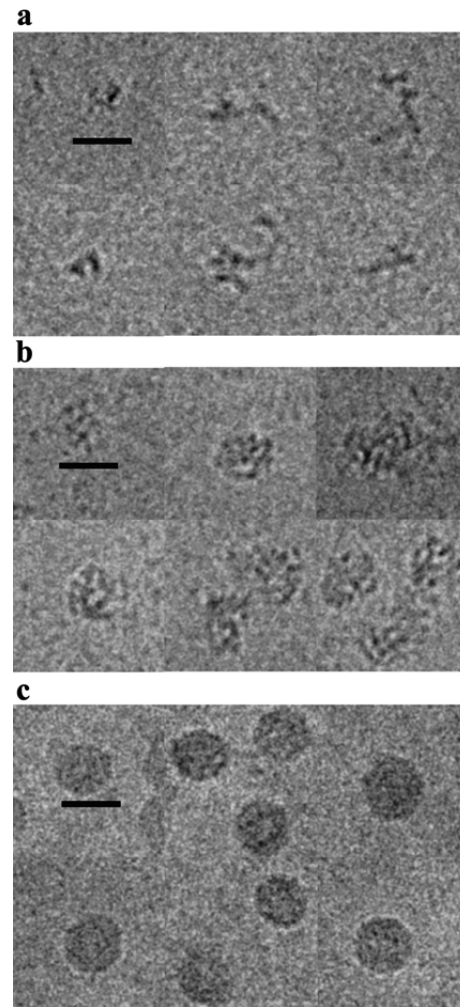


Figure 1. Cryo-electron micrographs of the assemblies at neutral pH and after acidification. (a) Pure 500-nt RNA. (b) At a CP:RNA mass ratio of 6:1 and neutral pH, CP/RNA complexes are amorphous and their electron density is low compared to that of properly formed VLPs; however, their size and shape are close to those of a capsid. (c) It is only upon pH acidification of the 6:1 solution of complexes that proper capsids (VLPs) are formed. The scale bar is 28 nm.

The unpackaged RNA in RNA assembly buffer (RAB, pH 7.2) is seen in Figure 1a; it exhibits the low electron density and irregular shapes similar to those seen in longer RNAs.²⁰ Its size, which we characterize by determining the geometric mean of the sides of a rectangle that contains all of the electron density, is ≈ 21 nm. When the RNA is mixed under these conditions with CP at a CP:RNA mass ratio of 6:1, the so-called magic ratio at which all of the RNA is packaged,⁷ irregular amorphous

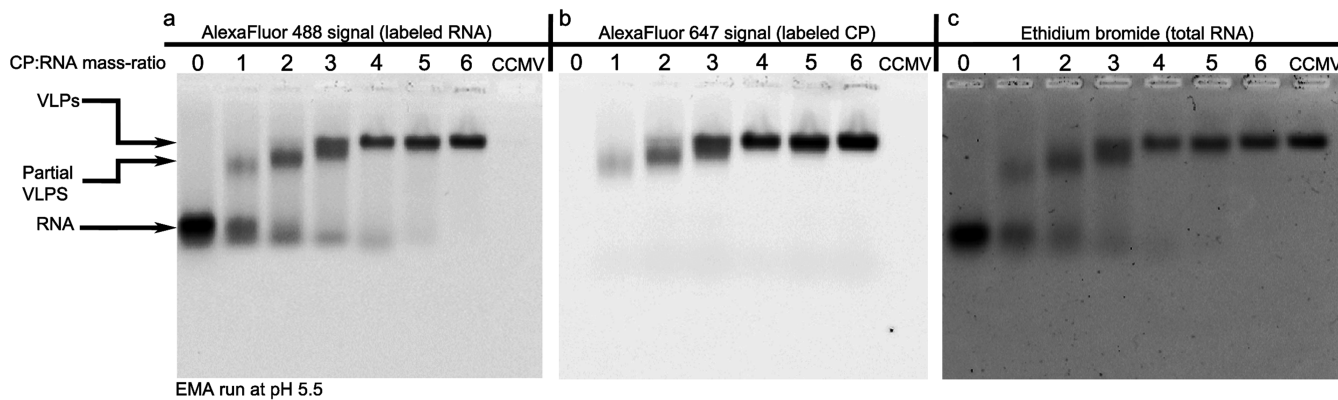


Figure 2. Electrophoretic mobility assays of 500-nt RNA with different amounts of CCMV CP demonstrating highly cooperative formation of nucleocapsids. 1% agarose EMA run at pH 5.5 and visualized by exciting either (a) fluorescently labeled RNA (AF488), (b) fluorescently labeled CP (AF647), or (c) stained RNA (ethidium bromide). A constant amount of AF488–500-nt RNA was titrated with AF647–CP, and the samples were assembled with the two-step protocol described in the text. Going from left to right, the mass ratio of CP:RNA in each lane increases from 0:1 to 6:1. These gels show that the 500-nt RNA capsid assembly is highly cooperative and that the minimum CP:RNA mass ratio at which all the RNA is packaged is 6:1 (*magic ratio*).

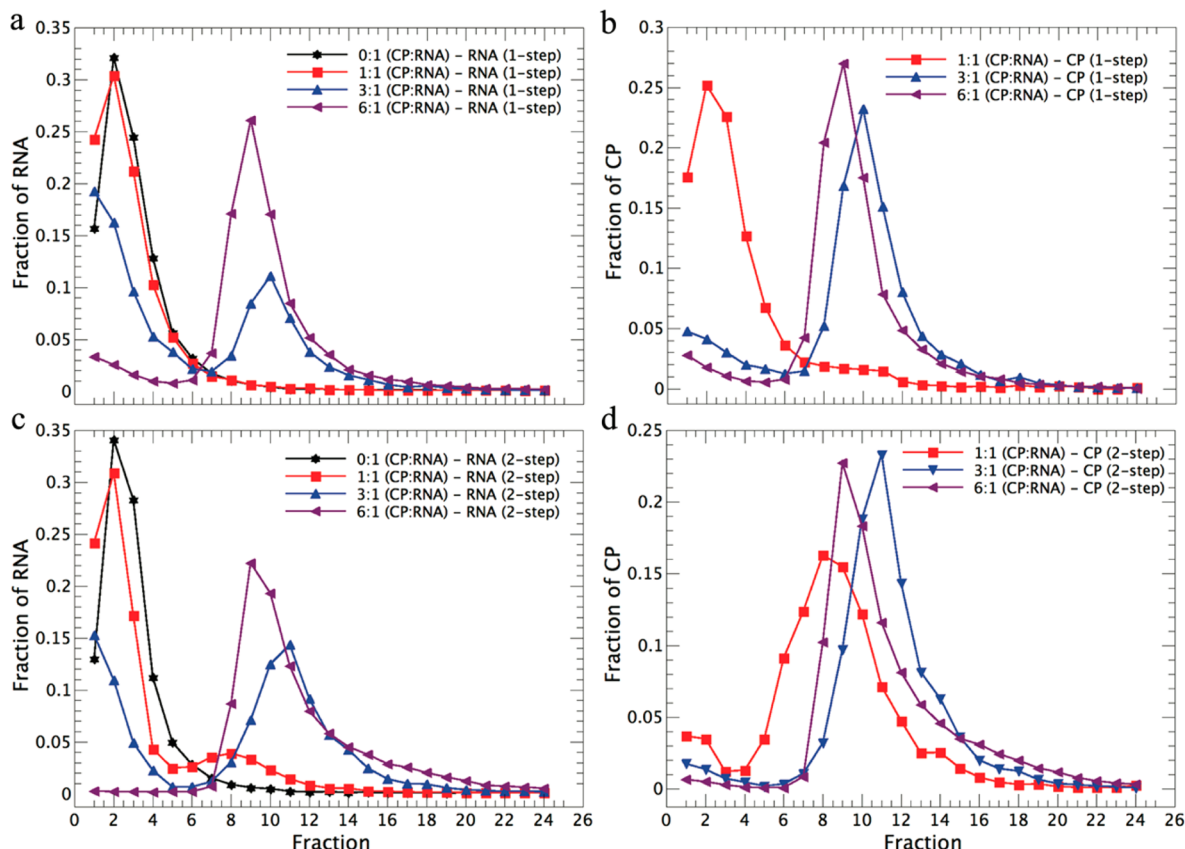


Figure 3. 500-nt RNAs form multiple-RNA complexes at neutral pH. Sedimentation profiles in a sucrose gradient of bilabeled assemblies (AF647–CP and AF488–RNA) at CP:RNA mass ratios of 0:1, 1:1, 3:1, and 6:1. (a and b) Profiles of the RNA (a) and CP (b) for the one-step assembly protocol. (c and d) Sedimentation profiles of the RNA (c) and CP (d) for the two-step assembly protocol. These sedimentation results show that, even at neutral pH, CP–RNA equilibrium involves only two species: single- and multi-RNA CP/RNA complexes.

complexes form that have a greater electron density than pure RNA and a diameter ≈ 22 nm. It is only upon acidification of these complexes that proper capsids are formed. Their size is comparable to that of a $T = 2$ structure, consistent with the sizes of capsids that have been found to be formed for RNAs ≤ 1000 nts in length.⁷ Note that in this paper we will reserve the term VLP for such regular and protective structures and use the

term multi-RNA complexes (MRCs) to refer to the amorphous complexes that are observed at neutral pH.

The assembly of CCMV CP around RNAs with lengths comparable to that of the WT (3000 nt's) or longer has been found to be noncooperative.^{7–10,13,14} As evident from the EMA shown in Figure 2, however, this is not the case for the 500-nt RNA. This titration gel shows the products of the two-step assembly protocol: 12 h dialysis against RAB followed by 12 h

dialysis against VSB, pH 4.5. Both components have been fluorescently labeled, allowing independent determination of the distribution of RNA (Figure 2a) and CP (Figure 2b) among the bands. The lanes are identified by the CP:RNA mass ratios, ranging from 0 to 6; WT CCMV virions are run in the rightmost column of all the gels but are apparent only in the one labeled with ethidium bromide (Figure 2c). At mass ratios <3 , there are two bands, one for RNA and another which can be attributed to a partially formed VLP; at ratios >3 , there is a small amount of free RNA and VLPs, which run in the same position as WT CCMV. (It should be noted that it has been demonstrated²¹ that the electrophoretic mobility of CCMV is characteristic only of its surface charge density. Since the ratio of charge/area for $T = 2$ and $T = 3$ capsids is identical, we expect that VLPs and WT CCMV will run similarly. While this dependence only on surface properties is appropriate to closed shells, it is not applicable to other structures, such as partially assembled capsids, so it is not possible to deduce their size from their band position.) In accord with our previous results,⁷ the minimum CP:RNA mass ratio required to package all of the RNA into VLPs is 6:1.

To determine if this highly cooperative behavior could be caused by a rapid change in pH that occurs when the assembly mixture is loaded into the gel (the EMA is run at pH 5.5), we dialyzed the assemblies only against RAB. This titration curve shows the same cooperative behavior at CP:RNA > 3 ; however, at lower mass ratios, there are more than two species (see Figure S1 in the Supporting Information), suggesting that at a low density of CP binding a rapid change in pH is not effective in reorganizing the CP.

The cooperative nature of the assembly is shown clearly by sedimentation profiles in sucrose gradients; moreover, such studies allow us to examine the difference between assemblies carried out only at neutral pH (one-step) and those in which there is a lowering of the pH (two-step). (An analysis of one-step assemblies with EMA is difficult because the quality of gels run at high pH is poor.) As with the EMAs, fluorescence labeling of the RNA and CP facilitates the analysis. One-step assemblies were carried out at CP:RNA mass ratios ranging from 0:1 to 6:1 and the products run in 10–40% sucrose gradients at pH 7.2. The fractions of the total RNA fluorescence within each eluted fraction for pure RNA and for the 1:1, 3:1, and 6:1 ratios are shown in Figure 3a. (For clarity, the distributions for the other ratios have not been shown; they can be found in Figure S2, Supporting Information.) At a 1:1 ratio, the RNA density distribution differs little from that for pure RNA. In contrast, at a 3:1 ratio, there is a marked decrease of the uncomplexed RNA in the top fractions and the appearance of a distinct species centered at the 10th fraction. The distributions of CP shown in Figure 3b parallel those in RNA. At 1:1, there is only a small shoulder, probably associated with a small amount of RNA/CP complex, while at 3:1 the peak in the CP profile at the 10th fraction demonstrates colocalization of CP and RNA, clear evidence of a complex. At 6:1, the magic ratio, almost 10% of the RNA remains in the top fractions, with the rest localized at fraction 9, where there is a corresponding peak in the CP. It is worth noticing that for the two-step assembly at 6:1 no free RNA is detected. The presence of only two species for all the ratios demonstrates the cooperativity of the assembly.

The multi-RNA nature of the complex can be understood by a comparison between the sedimentation studies for the one- and two-step assemblies. We have previously shown⁷ that two-

step assemblies at the magic ratio around 500-nt RNA lead to capsids that have 260 nm/280 nm absorbance ratios associated with the packaging of a total of 2000 nts of RNA in a $T = 2$ capsid, i.e., four RNAs. Consistent with this, the identical locations of the RNA and CP peaks for the 6:1 CP/RNA ratios in parts a,c and b,d of Figure 3, respectively, suggest that the RNA/CP complexes that assemble at neutral pH contain four RNAs. To confirm this, we have carried out sm-FCS studies of the assembly from which the number of encapsulated RNAs can be determined with precision.

The interaction of CP and RNA can also be seen in Figure 4, which shows the fractions of RNA and CP bound in the MRC

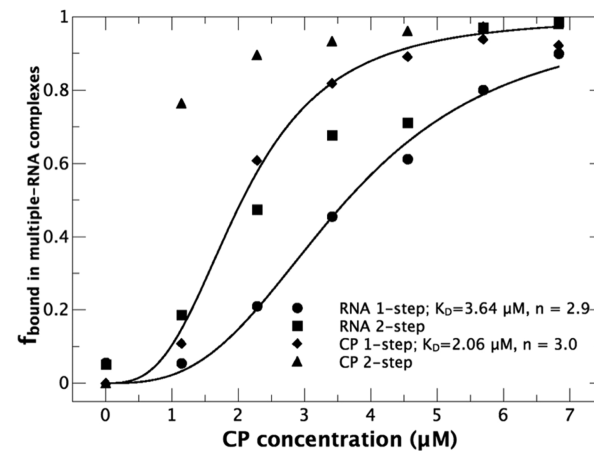


Figure 4. Equilibrium of CP between single-RNA and multiple-RNA complexes is cooperative at neutral pH. The fractions of CP and RNA in the multiple-RNA CP/RNA complexes were obtained by integration of the data in Figure 3. Only the fractions for the one-step assembly (where protein/RNA interactions are reversible) are then fitted to the Hill equation, to obtain the dissociation constant (K_D) and the Hill coefficient (n) for the equilibrium of the CP (or RNA) between the single- and MRCs. The Hill coefficient indicates not only the degree of cooperativity but also the minimum number of subunits of the substrate, in this case $n \approx 3$ for the one-step assembly. The solid lines show the Hill equation fits.

as a function of CP:RNA ratio, for one- and two-step assemblies. The four plots have been obtained by integrating the areas under the distributions from fractions 7–16 for the MRCs in Figure 3. It is evident from Figure 4 that the binding to the MRCs is highly cooperative and that it is only upon acidification that all of the RNA can be packaged if the CP:RNA mass ratio is 6:1. The behavior is similar to that in which small ligands bind to a substrate or to the association of monomers and which can be fitted to a Hill equation from which a binding constant and a degree of cooperativity can be obtained. Here, however, such an analysis is problematic because we have a combination of *coupled* processes involving protein binding to RNAs and association of protein-bound RNA complexes. More explicitly, the plots in Figure 4 for the CP do not simply correspond to equilibrium between free and bound CP but rather to that between CPs bound to a single RNA and ones in a multiple-RNA complex. Similarly, the curves for the RNA do not describe the association of naked RNAs but rather that between single- and multiple-RNA complexes induced by the CP. Nevertheless, if we use the Hill equation to fit Figure 4 data for the one-step assemblies (where protein/RNA interactions are reversible), we obtain K_D values

of $2.06 \mu\text{M}$ (CP) and $3.85 \mu\text{M}$ (RNA) and in both cases a Hill coefficient of 3.

sm-FCS Confirms That Acidification Is Required for VLP Formation. The self-assembly, velocity sedimentation, and EMA experiments all require relatively high RNA absolute concentrations (150 nM RNA). Accordingly, we used sm-FCS to estimate the size of the CP/RNA complexes at concentrations (10 nM RNA) that are more appropriate for comparison to the *in vivo* scenario.^{22,23} As discussed in the Supporting Information, measurements of the autocorrelation function, $G(\tau)$, can be analyzed to determine the size of a particle [hydrodynamic radius (R_h)], the number of particles in the confocal volume ($\langle N \rangle$), and the photophysics of the fluorophores. Since at any given time there are only a few ($\sim 1-5$) molecules in the fL confocal volume, artifacts due to aggregation are suppressed. Moreover, by labeling the RNA and the CP with different fluorophores, the size of each can be separately measured in the presence of the other.

Figure 5a shows the average R_h of AF488–RNA as a function of the amount of CP added to a fixed amount of RNA. To investigate the role of pH, we examined one- and two-step assemblies. We see that in both cases the R_h of AF488–RNA increases as the CP:RNA mass ratio increases. For the neutral-pH assembly (one-step), it rises essentially continuously from ~ 2.5 to ~ 6 nm, whereas in the two-step dialysis the R_h of the capsids levels off to about 11.0 nm at a mass ratio of 3 (note that the expected R_h for a $T = 2$ capsid is 11.5 nm). While the two-step data are in agreement with the density gradient fractionations in Figure 3, which show that at this ratio most of the RNA has formed VLPs, the sm-FCS results for the one-step assembly show that the RNA and CP associate only weakly, whereas the density gradients show that most of the RNA is found in the MRCs. This result points to the fact that the low concentrations used in the FCS studies ($0.4 \mu\text{M}$ CP) lie below the dissociation constant of the MRCs ($2-3 \mu\text{M}$ CP).

The gels also show that for the two-step assemblies there are only two species at any given mass ratio smaller than 6. We therefore tried to analyze the sm-FCS data for both assembly protocols by assuming that there were either one or two species in solution. Different choices of fitting assumptions (i.e., assuming one or two species), however, did not lead to significant changes in the R_h distributions (data not shown). Also, neither by keeping the R_h of one species constant while fitting the R_h and the mole fraction of the other species nor by fitting both R_h 's while keeping the mole fractions of the two species constant were we able to demonstrate that samples at a mass ratio ≥ 3 had a bimodal distribution around 2.5 and 11.5 nm, as one would expect from the EMA.

The failure to resolve two species is in accord with the analysis by Meseth and co-workers²⁴ who have shown that in order to measure a bimodal distribution in a two-component system by sm-FCS the ratio of the R_h 's for the species has to be greater than 1.6 and their mole fractions and quantum yields have to be comparable. In our experiments, two of these three criteria have been met: more explicitly, from Figures 2, 3, and S1 (Supporting Information), we see that at a CP:RNA mass ratio of 3 the mole fractions of single- and MRCs in the two-step assembly mixes are comparable, and from Figure 5a, we see at least a 3-fold difference in R_h 's for the single and multiple RNA/CP complexes. However, there is a 5-fold decrease in the quantum yield of fluorescently labeled RNA upon encapsidation (data not shown). This difference in quantum yields is therefore the most likely reason that we are unable to show

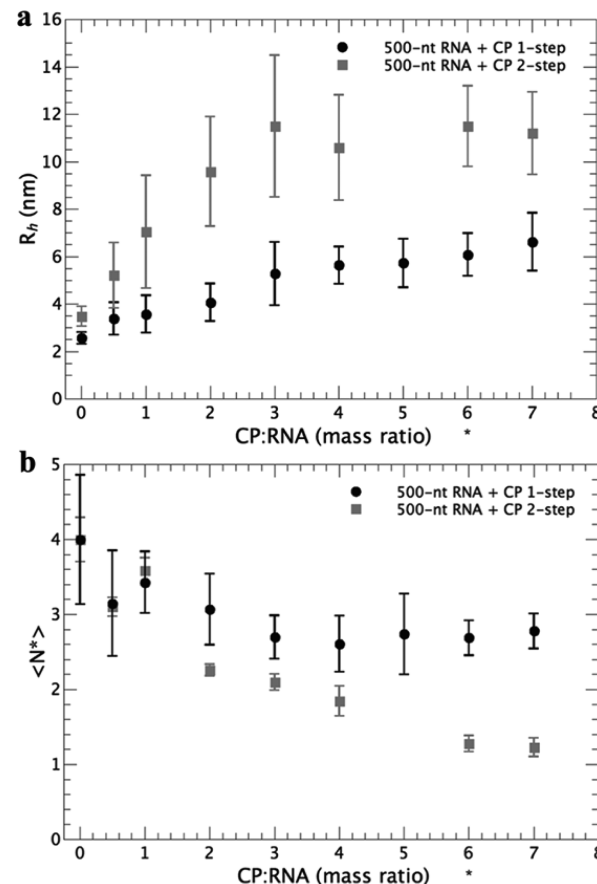


Figure 5. AF488-labeled 500-nt RNA hydrodynamic radii (R_h) and average number of particles ($\langle N^* \rangle$) as a function of added CP. (a) The R_h was obtained by fitting the sm-FCS $G(\tau)$ for AF488-labeled RNAs. The black circles and gray squares indicate, respectively, samples prepared by a one- and two-step protocol. The small increase in R_h at neutral pH demonstrates that CP/RNA complexes associate only weakly at neutral pH (one-step) and that acidification (two-step) is required to produce VLPs. The star on the x -axis indicates the magic ratio. (b) The normalized average number, $\langle N^* \rangle$, of particles of RNA decreases by a factor of 4 when VLPs are formed at the magic ratio after lowering the pH. In other words, four 500-nt RNAs are packaged into a capsid.

from the FCS data that there are two species in solution for CP:RNA mass ratios ≥ 3 and at low pH.

The average number of particles in the confocal volume, $\langle N \rangle$, can be calculated—see eq 2 in the Supporting Information—by extrapolating the autocorrelation function to $\tau = 0$. Figure 5b shows the average number of particles, $\langle N^* \rangle$, with respect to the value in the absence of CP, taken as 4. We see that for the one-step assemblies $\langle N^* \rangle$ decreases from about 4 to about 3 as the mass ratio increases from 0:1 to 6:1. In contrast, it decreases to 1 in the two-step assemblies. This result indicates that at the magic ratio and low pH (two-step assembly) four RNAs are packaged per VLP: it is only at CP:RNA = 0:1 (i.e., only for the case of RNA but no CP in solution) at both pHs, and at 6:1 at low pH, that $\langle N^* \rangle$ corresponds to a single diffusing species—naked RNA, or MRCs, respectively. In agreement with the titration gels at any other composition, in both one- and two-step assemblies, there are two species in solution—single-RNA CP/RNA complexes and MRCs.

While we were not able to determine the R_h 's of the two diffusing species by fitting the $G(\tau)$, it was straightforward to

deduce their $\langle N^* \rangle$ at low pH. As already noted, the quantum yield of the RNA in the VLPs is a factor of 5 lower than that of pure labeled RNA; by taking this into account in eq S7 (Supporting Information) and extrapolating to $\tau = 0$, we were able to show that 55% of the RNA is in the form of MRCs at CP:RNA = 3.

At neutral pH and at any mass ratio ≥ 3 , $\langle N^* \rangle$ remains constant. If we assume that both species have the same quantum yield and that the MRCs contain two RNAs (based on their R_h 's, which unlike closed-shell structures scale with the number of RNAs), we infer that 65% of the RNAs are in two-RNA/CP complexes. If the fluorescence quantum yield in the MRCs is as low as it is in VLPs, the analysis indicates that only 40% of the RNAs is present as two-RNA/CP complexes. Note that, even though at low pH the R_h does not change after a mass ratio of 3 (see Figure 5a), $\langle N^* \rangle$ reaches its minimum only at the magic ratio. This is possible only if at CP:RNA ≤ 5 there is still unpackaged RNA, which is in agreement with Figures 2, 3, and S1 (Supporting Information). It also confirms that a CP:RNA mass ratio of 6:1 is the minimum mass ratio required to package all of the RNA in solution.

To investigate if the final size of the capsid depends on the initial absolute concentration of 500-nt RNA, we carried out assemblies at the magic ratio by the two-step dialysis pathway at RNA concentrations of 50, 150, and 500 nM. The size distributions in Figure S3 (Supporting Information) obtained from negative-stain EM show that there are no significant differences in size between the VLPs formed at these three concentrations.

■ DISCUSSION

We have characterized the assembly of CCMV capsid protein around a short (compared to WT) ssRNA and have shown how it depends on pH, absolute concentration of RNA, and relative concentration of CP, i.e., the mass ratio CP:RNA. The special value of 6 for CP:RNA, referred to as the “magic ratio”, is the threshold for packaging all of the RNA. We have found that (i) at neutral pH the number of RNAs in the multiple-RNA CP/RNA complexes depends on the absolute concentration of RNA; (ii) four RNAs are encapsidated when VLPs are assembled in a two-step (neutral/pH 4.5) dialysis and at the magic ratio; (iii) the size of the capsid is independent of the absolute RNA concentration; (iv) at neutral pH, 150 nM RNA, and at CP:RNA mass ratios lower than the magic ratio, there are two species in solution—single CP-bound RNA molecules and MRCs; (v) the fraction of CP bound to the single-RNA CP/RNA complexes depends on the CP:RNA mass ratio, with this fraction always small compared to the fraction bound to the MRCs; and (vi) at neutral pH the multiple-RNA CP/RNA complexes (*protocapsids*) are amorphous even though their size and composition is similar to that of the final VLPs (at pH 4.5).

Nucleocapsid assembly for ssRNA viruses can be classified as either cooperative or noncooperative depending on whether at some CP concentration, lower than the minimum needed to package all of the RNA in solution, there are predominantly two (cooperative) or more species (noncooperative). Earlier work has suggested that cooperativity during capsid assembly is determined by the strength of the CP–CP interactions.^{14,25,26} Here we show that a CP exhibiting noncooperative assembly around “medium to large” (relative to genomic) RNAs^{7,14} can assemble into capsids with high cooperativity around small RNAs.

A similar conclusion has been reached in studies of the assembly of pentamers of SV40 VP1 around RNA,²⁶ where a shift in the degree of cooperativity was observed upon changing the length of the RNA. In the case of our results, the differences in length also represent differences in the numbers of RNAs packaged per capsid and it is likely that this is the controlling factor; i.e. (see discussion below), association of two or more CP-bound RNA complexes is responsible for the cooperative behavior. This appears not to be the case for RNA packaged in SV40, where cooperativity is observed both for 75-nt RNA— involving 2 molecules per capsid—and for 524-nt RNA— involving 1 molecule per capsid.²⁷

For our assemblies of CCMV CP and a 500-nt RNA, both the EMAs and the sucrose gradients show that at CP:RNA mass ratios $< 6:1$ there are two main species: single-RNA CP/RNA complexes (with a small amount of bound CP) and MRCs that have an excess of bound CP. By an excess of CP, we mean that there is more CP bound than the 120 required to form a $T = 2$ capsid. This superstoichiometric amount of bound CP has been shown to be essential for packaging all of the RNA in solution.⁷ Figure 3 shows that even in the two-step assemblies the excess CP is bound to the VLP. Hiebert and Bancroft²⁸ have noted that in assemblies carried out with excess protein an “extra coat” of CP could be formed. Experimental and theoretical studies of the self-assembly of CCMV CP in the absence of negatively charged cargo^{29–31} have shown as well that CCMV CP can spontaneously form *multi-shells* at low pH and medium ionic strength. This suggests that, during the pH-lowering step, the excess CP bound to the CP/RNA complexes first unbinds from the RNA, allowing capsid formation, and then binds to the exterior surface of the VLP. The partial second shells that result are seen clearly in Figure 6, in a 500

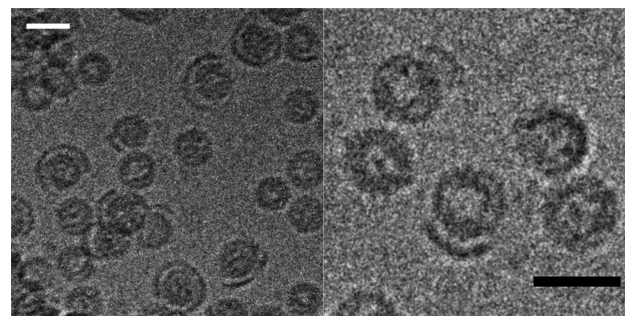


Figure 6. Cryo-electron micrographs of the assemblies after acidification. A small fraction of the capsids obtained by the two-step assembly protocol and at a CP:RNA mass ratio of 6:1 show partial second shells associated originating from the excess of CP in solution that is needed to package 100% of the RNA in solution. The scale bar is 25 nm.

nM RNA sample carried through the two-step assembly process at the magic ratio; it appears that a concentration of 150 nM is not sufficiently far above the critical micelle concentration for CP for the excess protein to be predominantly in the form of second shells. Note that the fact that we only observe single-RNA CP/RNA complexes and MRCs *but no free CP* (even at single-molecule concentrations) is in agreement with the *en masse* assembly mechanism described by Elrad and Hagan³² in which CP absorption onto the RNA proceeds to saturation, followed by desorption of CP as VLPs form. A similar scenario was proposed by Devkota et al.³³ for the nonspecific binding of CP tails to RNA, preceding collapse of the CP/RNA complex

and nucleocapsid formation. The work of Zhang and Linse³⁴ is the only simulation of which we are aware that considers polymer chains sufficiently short that several of them are packaged in the same capsid, but cooperativity of the process is not analyzed.

The sucrose gradient, EMA, and sm-FCS data for pure RNAs demonstrate that *in the absence of CP the RNA does not form dimers or multimers*; therefore, the association of two or more RNAs must be promoted by the binding of CP. Accordingly, the formation of MRCs is due to association of CP/RNA complexes, as opposed to association of CP-free (“naked”) RNAs.

There are two basic physical factors that allow us to understand how binding by CP drives the association of RNAs into MRCs of special sizes: lateral interactions between CPs that create an effective *line tension* and the *spontaneous curvature* of the CP shell. The line tension is associated with the fact that a patch of laterally interacting CPs is a two-dimensional domain with a high-energy boundary (due to missing nearest neighbors) that can be minimized by growth of the large patches at the expense of the smaller ones, in the classical sense of Ostwald ripening. This drives the association of CP-bound RNAs, and accounts for the asymmetry observed in the CP coverage on single- and MRCs, i.e., the fact that the data in Figure 4 for the CP and RNA do not overlap. Moreover, the larger the number of RNAs in an RNA–CP complex, the lower the free energy per CP because of the possibility of forming larger clusters of interacting CPs (i.e., minimizing surface [line] energy), therefore providing a driving force for both association of complexes and correspondingly higher CP coverage in the MRCs. Note that these effects are operative over the full pH range studied, because although weak compared to those at acidic pH,⁹ CCMV CP–CP lateral interactions are nevertheless operative at neutral pH.

The association of CP/RNA complexes is also controlled by the *curvature* with which CPs prefer to interact with one another. More explicitly, these interactions vary with the *angle* between two adjacent CPs, taking on minimal values for angles corresponding to the discretized curvatures corresponding to *T*-numbers in the Caspar–Klug hierarchy. In the case of CCMV, it appears that the *T* = 2 minimum is sufficiently low that a capsid can form with this curvature. Accordingly, at a sufficiently high concentration and/or a sufficiently low pH (to guarantee effective interactions between CPs, as described above), the CP/RNA complexes associate until enough of them (four) are present to stabilize the bound CPs with *T* = 2 curvature.

In a cooperative model, the first binding event has the lowest affinity, and large changes in ligand concentration are needed to promote ligand binding. Recall that by fitting the binding curves (Figure 4) we extracted a Hill coefficient of 3 for the equilibrium between single- and MRCs at neutral pH. Given that four RNAs are packaged, it is likely that the dimerization of CP/RNA complexes is the low-affinity event while the subsequent formation of three- and four-RNA/CP complexes are higher-affinity events. This model is consistent with the sm-FCS data at neutral pH, which show that even at the magic ratio—but at a CP concentration lower than K_D of the MRC for either the CP or RNA—the CP/RNA complexes are smaller in size than a VLP and have fewer than four RNAs. As shown in Figure 4b, $\langle N^* \rangle$ decreases from 4 to 3 when the CP:RNA mass ratio increases from 0:1 to 6:1, suggesting that at this concentration and mass ratio the interaction of CP/RNA

complexes leads to equilibrium between monomeric and dimeric CP/RNA complexes rather than to formation of a complex containing four RNAs.

A simple “all-or-nothing” model highlights the strong cooperativity of the actual nucleocapsid formation process that arises from coupling of the binding of CP to RNA (as evidenced by the formation of MRC) and the association of CP-bound RNAs with one another (that arises at low pH). More explicitly, CP binding to RNA is enhanced by lateral interactions between neighboring CPs, with this effect further enhanced by intercomplex association because of the formation of larger CP clusters (thereby minimizing surface energy) that also enjoy a larger radius of curvature (thereby minimizing bending energy).

Consider the limit of *perfect cooperativity*, i.e., for *any* CP:RNA ratio, binding of CP to an RNA results exclusively in saturated binding of that RNA with subsequent association of these saturated RNAs to form four-RNA nucleocapsids. Let x denote the CP:RNA mole ratio at which the self-assembly reaction is carried out, and let N denote the total number of RNAs in solution. Perfect cooperativity implies that CP will only be associated with saturated RNAs (each bound by electrostatic interactions with 50 CPs, each of which has an N-terminus with a charge of +10) and with VLPs with a *T* = 2 structure—hence composed of 120 copies of CP—and containing four RNAs. It follows that, for any x , the number of nucleocapsids formed will be the maximum possible, i.e., the number using all of the (xN) CPs available. Accordingly, there will be $xN/120$ capsids, corresponding to $4xN/120$ packaged RNAs (out of the original N in solution) and hence a fraction $(1/30)x$ of RNAs packaged. Figure 7 compares this result with the measured fraction of RNA packaged as a function of CP:RNA mole ratio (with data taken from the two-step RNA curve in Figure 4, replotted against the CP:RNA mole ratio rather than absolute CP concentration for fixed RNA

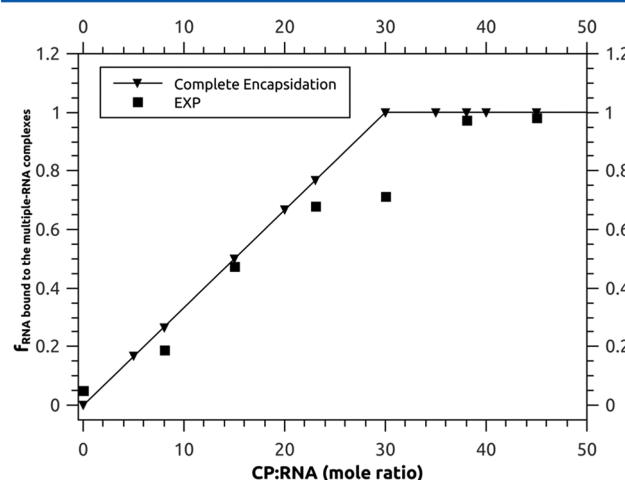


Figure 7. Fraction of RNA in virus-like particles for the case of perfect cooperativity of CP binding/RNA-complex association. Assuming saturation of CP binding on RNAs and consequent association of four of the resulting complexes, a fraction $(1/30)x$ of the RNA will be packaged (see discussion in text), where x is the CP:RNA ratio in the solution. Here we compare this result (inverted triangles) with the measured fraction of RNA packaged (squares) as a function of CP:RNA mole ratio, with data taken from the two-step RNA data in Figure 4, replotted here against CP:RNA mole ratio rather than absolute CP concentration for fixed RNA concentration.

concentration). The strong cooperativity of nucleocapsid formation is evident.

Note that even a 10-fold increase in the absolute concentration of RNA (while keeping the CP:RNA mass ratio constant) has no effect on the size of the capsid. It is known that CCMV CP has a preferred curvature involving a radius of 14 nm (corresponding to a $T = 3$ capsid), when CP assembles in the presence of WT-length RNA or in the absence of RNA. However, we find a VLP diameter consistent with that of $T = 2$ capsids, implying that the final size of the capsid depends on how the RNA (of a particular length) affects the preferred curvature of the bound CPs and not on the absolute RNA concentration.

Finally, our sm-FCS and cryo-EM data are in agreement with previous results^{7–9} showing that at neutral pH CCMV CP lateral interactions are too weak to nucleate the formation of a spherical shell; instead, formation of capsids requires a lowering of the pH. The need for a two-step dialysis pathway reinforces the conclusion that successful capsid assembly involves tuning of the CP–CP and CP–RNA interactions to minimize kinetic traps.

CONCLUSIONS

We are proposing a cooperative mechanism for the assembly of VLPs around short ssRNAs that highlights the role of the nucleic acid as a scaffold and as an active component in capsid assembly: (i) when CP and RNA are mixed at neutral pH, all of the CP is bound, even when CP is present at superstoichiometric concentrations; (ii) the formation of complexes consisting of two or more molecules of CP-bound RNA is driven by CP–CP interactions; (iii) the difference in the chemical potential of CP in single- and multiple-molecule RNA/CP complexes results in a two-state system at CP:RNA mass ratios less than 6:1, with the single-RNA species having a significantly lower density of bound CP; (iv) the formation of dimers of one-RNA CP/RNA complexes is the lowest affinity-binding step, while the formation of three- and four-RNA complexes is highly cooperative; and (v) the multiple-RNA CP/RNA complexes are not proper nucleocapsids unless the CP–CP interactions are increased by pH lowering.

ASSOCIATED CONTENT

Supporting Information

This section contains an analysis of the sm-FCS data, electrophoretic mobility assays under acidic conditions of one-step assembly products (demonstrating that a rapid change in pH is not enough to equilibrate CP/RNA complexes at low mass ratios), and electron micrographs of VLPs (showing that capsid size is independent of the absolute RNA concentrations). This material is available free of charge via the Internet at <http://pubs.acs.org>.

AUTHOR INFORMATION

Corresponding Author

*E-mail: gelbart@chem.ucla.edu.

Present Address

[†]HIV Drug Resistance Program, Center for Cancer Research, National Cancer Institute, Frederick, MD 21702.

Notes

The authors declare no competing financial interest.

ACKNOWLEDGMENTS

The FCS and electron microscopy measurements were carried out at the California NanoSystems Institute with the support of Dr. Laurent Bentolila, Dr. Matthew Schibler, and SangYoon Chung at the Advanced Light Microscopy and Spectroscopy facility and of Ivo Atanasov at the Electron Imaging Center for Nano-Machines. We thank Prof. Feng Guo for providing the T7 RNA polymerase and Prof. A. L. N. Rao for helpful discussions. This work was supported by the U.S. National Science Foundation, in the form of grant CHE 1051507 to W.M.G. and C.M.K., and by the Israel Science Foundation (ISF grant 1448/10) for financial support to A.B.-S. and S.W.S.

REFERENCES

- (1) Venter, P. A.; Krishna, N. K.; Schneemann, A. Capsid Protein Synthesis From Replicating RNA Directs Specific Packaging Of The Genome Of A Multipartite, Positive-Strand RNA Virus. *J. Virol.* **2005**, *79*, 6239–6248.
- (2) Bancroft, J. B. The Self-Assembly Of Spherical Plant Viruses. *Adv. Virus Res.* **1970**, *16*, 99–134.
- (3) Adolph, K. W.; Butler, P. J. G. Studies On The Assembly Of A Spherical Plant Virus. III. Reassembly Of Infectious Virions Under Mild Conditions. *J. Mol. Biol.* **1977**, *109*, 345–357.
- (4) Annamalai, P.; Rao, A. L. N. Dispensability Of 3' tRNA-Like Sequence For Packaging Cowpea Chlorotic Mottle Virus Genomic RNAs. *Virology* **2005**, *332*, 650–658.
- (5) Kobayashi, A.; Ehara, A. In Vitro Encapsulation Of Cucumber Mosaic Virus RNA Species. *Ann. Phytopathol. Soc. Jpn.* **1995**, *61*, 99–102.
- (6) Ford, R. J.; Barker, A. M.; Bakker, S. E.; Coutts, R. H.; Ranson, N. A.; Phillips, S. E. V.; Person, A. R.; Stockley, P. G. Sequence-Specific, RNA-Protein Interactions Overcome Electrostatic Barriers Preventing Assembly Of Satellite Tobacco Necrosis Virus Coat Protein. *J. Mol. Biol.* **2013**, *425*, 1050–1064.
- (7) Cadena-Nava, R. D.; Comas-Garcia, M.; Garmann, R. F.; Rao, A. L. N.; Knobler, C. M.; Gelbart, W. M. Self-Assembly Of Viral Capsid Protein And RNA Molecules Of Different Sizes: Requirement For A Specific High Protein/RNA Mass Ratio. *J. Virol.* **2012**, *86*, 3318–3326.
- (8) Comas-Garcia, M.; Cadena-Nava, R. D.; Rao, A. L. N.; Knobler, C. M.; Gelbart, W. M. In Vitro Quantification Of The Relative Packaging Efficiencies Of Single-Stranded RNA Molecules By Viral Capsid Protein. *J. Virol.* **2012**, *86*, 12271–12282.
- (9) Garmann, R. F.; Comas-Garcia, M.; Gopal, A.; Knobler, C. M.; Gelbart, W. M. The Assembly Pathway Of An Icosahedral Single-Stranded RNA Virus Depends On The Strength Of Inter-Subunit Attraction. *J. Mol. Biol.* **2014**, *426*, 1050–1060.
- (10) Rao, A. L. N. Genome Packaging By Spherical Plant RNA Viruses. *Annu. Rev. Phytopathol.* **2006**, *44*, 61–87.
- (11) Annamalai, P.; Rao, A. L. N. Packaging Of Brome Mosaic Virus Sub-Genomic RNA Is Functionally Coupled To Replication-Dependent Transcription And Translation Of Coat Protein. *J. Virol.* **2006**, *80*, 10096–10108.
- (12) Venter, P. A.; Schneemann, A. Assembly Of Two Independent Populations Of Flock House Virus Particles With Distinct RNA Packaging Characteristics In The Same Cell. *J. Virol.* **2007**, *81*, 613–619.
- (13) Fox, J. M.; Wang, G.; Speir, J. A.; Olson, N. H.; Johnson, J. E.; Baker, T. S.; Young, M. J. Comparison Of The Native CCMV Virion With In Vitro Assembled CCMV Virions By Cryoelectron Microscopy And Image Reconstruction. *Virology* **1998**, *244*, 212–218.
- (14) Johnson, J. M.; Willits, D. A.; Young, M. J.; Zlotnick, A. Interaction With Capsid Protein Alters RNA Structure And The Pathway For In Vitro Assembly Of Cowpea Chlorotic Mottle Virus. *J. Mol. Biol.* **2004**, *335*, 455–464.
- (15) Dreher, T. W.; Rao, A. L. N.; Hall, T. C. Replication In Vivo Of Mutant Brome Mosaic Virus RNAs Defective In Aminoacylation. *J. Mol. Biol.* **1989**, *206*, 425–438.

- (16) Sambrook, J.; Fritsch, E. F.; Maniatis, T. *Molecular cloning: a laboratory manual*; Cold Spring Harbor Laboratory Press: Cold Spring Harbor, NY, 1989.
- (17) Bancroft, J. B.; Hills, G. J.; Markham, R. A Study Of The Self-Assembly Process In A Small Spherical Virus Formation Of Organized Structures From Protein Subunits In Vitro. *Virology* **1967**, *31*, 354–379.
- (18) Gillitzer, E.; Willits, D.; Young, M. J.; Douglas, T. Chemical Modification Of A Viral Cage For Multivalent Presentation. *Chem. Commun.* **2002**, *20*, 2390–2391.
- (19) Tsay, J. M.; Doose, S.; Weiss, S. Rotational And Translational Diffusion Of Peptide-Coated [1] CdSe/CdS/ZnS Nanorods Studied By Fluorescence Correlation Spectroscopy. *J. Am. Chem. Soc.* **2006**, *128*, 1639–1647.
- (20) Gopal, A.; Zhou, H. Z.; Knobler, C. M.; Gelbart, W. M. Visualizing Large RNA Molecules In Solution. *RNA* **2012**, *18*, 284–299.
- (21) Vega-Acosta, J. R.; Cadena-Nava, R. D.; Gelbart, W. M.; Knobler, C. M.; Ruiz-Garcia, J. Electrophoresis Mobilities of a Viral Capsid, Its Capsid Protein, and Their Relation to Viral Assembly. *J. Phys. Chem. B* **2014**, *118*, 1984–1989.
- (22) Beckett, D.; Wu, H. N.; Uhlenbeck, O. C. Roles Of Operator And Non-Operator RNA Sequences In Bacteriophage R17 Capsid Assembly. *J. Mol. Biol.* **1988**, *204*, 939–947.
- (23) Borodavka, A.; Tuma, R.; Stockley, P. G. A Two-Stage Mechanism Of Viral RNA Compaction Revealed By Single Molecule Fluorescence. *RNA Biol.* **2013**, *10*, 1–9.
- (24) Meseth, U.; Wohland, T.; Rigler, R.; Vogel, V. Resolution Of Fluorescence Correlation Measurements. *Biophys. J.* **1999**, *76*, 1619–1631.
- (25) Zlotnick, A.; Porterfield, J. Z.; Wang, C.-Y. To Build A Virus On A Nucleic Acid Substrate. *Biophys. J.* **2013**, *104*, 1595–1604.
- (26) Porterfield, J. Z.; Dhason, M. S.; Loeb, D. D.; Nassal, M.; Stray, S. J.; Zlotnick, A. Full-Length Hepatitis B Virus Core Protein Packages Viral And Heterologous RNA With Similarly High Levels Of Cooperativity. *J. Virol.* **2010**, *84*, 7174–7184.
- (27) Kler, S.; Wang, C.-Y. J.; Ohason, M.; Oppenheim, A.; Zlotnick, A. Scaffold Properties Are A Key Determinant Of The Size And Shape Of Self-Assembled Virus-Derived Particles. *ACS Chem. Biol.* **2013**, *8*, 2753–2761.
- (28) Hiebert, E.; Bancroft, J. B. Factors Affecting the Assembly of Some Spherical Viruses. *Virology* **1969**, *39*, 296–311.
- (29) Adolph, K. W.; Butler, P. J. G. Studies On The Assembly Of A Spherical Plant Virus. I. States Of Aggregation Of The Isolated Protein. *J. Mol. Biol.* **1974**, *88*, 327–338.
- (30) Lavelle, L.; Cadena-Nava, R. D.; Gingery, M.; Vega-Acosta, J. R.; Phillips, M.; Pinedo-Torres, L. A.; Ruiz-Garcia, J.; Gelbart, W. M.; Knobler, C. M. Phase Diagram Of Self-Assembled Viral Capsid Protein Polymorphs. *J. Phys. Chem. B* **2009**, *113*, 3813–3820.
- (31) Prinsen, P.; van der Schoot, P.; Gelbart, W. M.; Knobler, C. M. Multishell Structures Of Virus Coat Proteins. *J. Phys. Chem. B* **2010**, *114*, 5522–5533.
- (32) Elrad, O. M.; Hagan, M. F. Encapsulation Of A Polymer By An Icosahedral Virus. *Phys. Biol.* **2010**, *7*, 045003.
- (33) Devkota, B.; Petrov, A. S.; Lemieux, S.; Boz, M. B.; Tang, L.; Schneemann, A.; Johnson, J. E.; Harvey, S. C. Structural And Electrostatic Characterization Of Pariacoto Virus: Implication For Viral Assembly. *Biopolymers* **2009**, *91*, 530–538.
- (34) Zhang, R.; Linse, P. Icosahedral capsid formation by capsomers and short polyions. *J. Chem. Phys.* **2013**, *138*, 1549011–1549014.